Available online at www.sciencedirect.com
SCIENCE DIRECT®
Journal of Sound and Vibration 270 (2004) 729–753
JOURNAL OF SOUND AND VIBRATION
www.elsevier.com/locate/jsvi

Dynamic response of rotating beams with piezoceramic actuation

Dipali Thakkar*, Ranjan Ganguli

Department of Aerospace Engineering, Indian Institute of Science, Bangalore 560012, India

Received 11 June 2002; accepted 4 February 2003

Abstract

The dynamic behaviour of rotating beams with piezoceramic actuation is studied using bending (d_{31}) and shear (d_{15}) actuation for application to structures such as helicopter and wind turbine rotor blades. The governing equations are derived using Hamilton's principle for a beam undergoing transverse bending, inplane bending, torsion and axial deformations. The effect of moderate deflections are included by retaining non-linear terms. The equations are then solved using finite element discretization in the spatial and time domain. Results are obtained for the cases with only actuation loads, with actuation loads and added periodic tip loads, and for a pretwisted beam. Numerical results show that the centrifugal stiffening effect reduces the tip transverse bending deflection and elastic twist obtained from smart actuation as the rotation speed increases. However, the effect of rotation speed on the tip elastic twist is less pronounced. The importance of non-linear terms for accurate prediction of torsion, in-plane bending and transverse bending response is also shown. It is also found that combinations of pretwist and smart actuation can be used to obtain desirable torsion response over a range of rotation speeds.

1. Introduction

The emerging area of smart materials and structures offers novel solutions to vibration problems. Smart structures is also known as active-materials technology. A smart structure is a combination of actuators, sensors and microprocessors. Common materials used for such structures are piezoelectric, electrostrictive, magnetostrictive and shape memory alloys. Among these materials, piezoelectrics have found increasing use for aerospace structures [1,2].

Piezoelectric materials such as lead zirconate titanate (PZT), have the capability of undergoing strain on the application of an electric field. This concept is known as converse piezoelectric effect

*Corresponding author.
E-mail addresses: dipali@aero.iisc.ernet.in (D. Thakkar), ganguli@aero.iisc.ernet.in (R. Ganguli).

0022-460X/03/$ - see front matter
doi:10.1016/S0022-460X(03)00189-5

and is exploited in actuators. It allows the alteration of system characteristics as well as the system response [3]. The same material (PZT) generates electric charge when subjected to mechanical force or deformation. This is known as the direct piezoelectric effect and is used in sensors. The microprocessors analyze the response from the sensors and use distributed parameter control theory to command the actuators to apply localized stresses to minimize the response of the system.

Considerable work has been done on the modelling of beams with piezoelectric actuators [4–10]. However, this literature addresses modelling of non-rotating beams. Helicopter and wind turbine blades are rotating beam type structures. Because of the importance of such structures, work has been done in the dynamic analysis of rotating beams [11–16]. However, only a few studies have been done in the dynamic analysis of rotating smart beams [17–19]. In Refs. [17,18], authors place piezoceramic actuators at $\pm 45^\circ$ on the top and bottom of the beam to induce torsion actuation. However, for slowly rotating structures such as wind turbines, bending actuation may also be useful.

The governing non-linear equations of motion for the elastic bending and torsion of twisted non-uniform rotor blades made of isotropic material were derived by Hodges and Dowell [20] using the Hamilton's principle and have become the underlying basis for comprehensive aeroelastic analysis developed and used by several researchers [21–24]. Geometrical non-linearities, which result from moderate blade deflections, play an important role in the aeroelastic stability analysis of rotor blades. Generally, moderate deflection type theories based on an ordering scheme are quite adequate for hingeless rotor blades. However, large deflection theories can be important for the bearingless rotors [25]. In this paper, we extend the analysis in Ref. [20] to include rotating beams with piezoceramic actuation. The governing equations for rotating smart beams are derived and numerical results are obtained to analyze the influence of smart actuation, centrifugal stiffening, non-linear effects and pretwist. The possibility of using the piezoceramic shear actuation mechanism (d_{15} effect) for torsion and the bending actuation (d_{31} effect) for bending of rotating beams is explored. The d_{15} effect is being recently used by some researchers [26–28]. It should be noted that small amount of deflections can be used to reduce airloads and evolve an active control strategy for rotating beam type structures.

2. Formulation

In this section, the governing equations of a smart rotating beam are derived, the solution procedure is discussed and the smart structure terms in the equations are identified.

2.1. Structural modelling

The constitutive equations of an isotropic beam plate [29] can be written as follows:

$$\begin{Bmatrix} \varepsilon_{xx} \\ \varepsilon_{\eta\eta} \\ \varepsilon_{\zeta\zeta} \\ \gamma_{x\eta} \\ \gamma_{\eta\zeta} \\ \gamma_{x\zeta} \end{Bmatrix} = \begin{bmatrix} 1/E & -\nu/E & -\nu/E & 0 & 0 & 0 \\ -\nu/E & 1/E & -\nu/E & 0 & 0 & 0 \\ -\nu/E & -\nu/E & 1/E & 0 & 0 & 0 \\ 0 & 0 & 0 & 1/G & 0 & 0 \\ 0 & 0 & 0 & 0 & 1/G & 0 \\ 0 & 0 & 0 & 0 & 0 & 1/G \end{bmatrix} \begin{Bmatrix} \sigma_{xx} \\ \sigma_{\eta\eta} \\ \sigma_{\zeta\zeta} \\ \tau_{x\eta} \\ \tau_{\eta\zeta} \\ \tau_{x\zeta} \end{Bmatrix} \tag{1}$$

The induced strains [30] for a piezoelectric material poled in $(z, 3)$ direction can be written as

$$\begin{Bmatrix} \Lambda_{xx} \\ \Lambda_{\eta\eta} \\ \Lambda_{\zeta\zeta} \\ \Lambda_{\eta\zeta} \\ \Lambda_{x\zeta} \\ \Lambda_{x\eta} \end{Bmatrix} = \begin{bmatrix} 0 & 0 & d_{31} \\ 0 & 0 & d_{31} \\ 0 & 0 & d_{33} \\ 0 & d_{15} & 0 \\ d_{15} & 0 & 0 \\ 0 & 0 & 0 \end{bmatrix} \begin{Bmatrix} E_1 \\ E_2 \\ E_3 \end{Bmatrix}, \tag{2}$$

where Λ is the induced strain, d_{31}, d_{15}, and d_{33} are piezoelectric strain coefficients and E_1, E_2 and E_3 are the electric fields in $(x, 1)$, $(y, 2)$ and $(z, 3)$ directions, respectively.

The following fundamental assumptions are made for the analysis [20]:

(i) Mid-line of a plate segment does not deform in its own plane, meaning that the in-plane warping of the cross-section is neglected;
(ii) the normal stress in the contour direction, $\sigma_{\eta\eta}$ is neglected relative to the normal axial stress σ_{xx} and
(iii) rotor blade is a long slender beam and hence the uniaxial stress assumptions can be made; $\sigma_{\eta\eta} = 0$, $\sigma_{\zeta\zeta} = 0$ and $\tau_{\eta\zeta} = 0$.

The strain–displacement field (accurate up to second order and accounting for moderate deflections) is defined as [20]

$$\varepsilon_{xx} = u' + \frac{v'}{2} + \frac{w'^2}{2} - \lambda_T\phi'' + (\eta^2 + \zeta^2)(\theta_0'\phi' + \phi'^2/2) - v''[\eta\cos(\theta_0 + \hat{\phi}) - \zeta\sin(\theta_0 + \hat{\phi})] - w''[\eta\sin(\theta_0 + \hat{\phi}) + \zeta\cos(\theta_0 + \hat{\phi})], \tag{3}$$

$$\varepsilon_{x\eta} = -(\zeta + \lambda_{T,\eta})\phi' = -\hat{\zeta}\phi', \tag{4}$$

$$\varepsilon_{x\zeta} = (\eta - \lambda_{T,\zeta})\phi' = \hat{\eta}\phi', \tag{5}$$

where u, v, w and $\hat{\phi}$ are axial, chord-wise bending, span-wise bending and elastic twist, respectively, θ_0 is the blade pitch and η and ζ are cross-sectional co-ordinates and λ_T is the cross-sectional warping function. Also $\hat{\phi}' = \phi' - w'v''$ and $u = u_e - \frac{1}{2}\int_0^x (v'^2 + w'^2)\,\mathrm{d}x$.

Based on these assumptions and strain-displacement relationships (Eq. (3) to Eq. (5)), Hamilton's principle is used to derive the system of equations of motion. For a conservative system, it states that the true motion of a system, between prescribed initial conditions at time ψ_1 and final conditions at time ψ_2, is that particular motion for which the time integral for the difference between potential and kinetic energies is a minimum. The generalized Hamilton's principle applicable to non-conservative systems is expressed as

$$\delta\Pi = \int_{\psi_1}^{\psi_2} (\delta U - \delta T - \delta W)\,\mathrm{d}\psi = 0, \tag{6}$$

where δU, δT and δW are virtual variations of strain energy, kinetic energy and virtual work done by external force, respectively and $\delta\Pi$ represents the total potential of the system. The strain

Table 1
Isotropic and smart material contributions to strain energy

Isotropic terms	Smart terms
$\delta U_1 = \int_v E\varepsilon_{xx}\delta\varepsilon_{xx}\,\mathrm{d}v$	$\delta U_{S_1} = \int_v Ed_{31}E_3\delta\varepsilon_{xx}\,\mathrm{d}v$
$\delta U_2 = \int_v G\varepsilon_{x\eta}\delta\varepsilon_{x\eta}\,\mathrm{d}v$	$\delta U_{S_2} = \int_v Gd_{15}E_2\delta\varepsilon_{x\eta}\,\mathrm{d}v$
$\delta U_3 = \int_v G\varepsilon_{x\zeta}\delta\varepsilon_{x\zeta}\,\mathrm{d}v$	$\delta U_{S_3} = 0$
$\delta U_{iso} = \delta U_1 + \delta U_2 + \delta U_3$	$\delta U_{smart} = \delta U_{S_1} + \delta U_{S_2} + \delta U_{S_3}$
Total $= \delta U_{iso} + \delta U_{smart}$	

energy of the system can be written as follows:

$$U = \frac{1}{2}\int_0^R \int_A \int (\sigma_{xx}\varepsilon_{xx} + \sigma_{x\eta}\varepsilon_{x\eta} + \sigma_{x\zeta}\varepsilon_{x\zeta})\,\mathrm{d}\eta\,\mathrm{d}\zeta\,\mathrm{d}x \tag{7}$$

and divided into isotropic and smart components as shown in Table 1. Bending actuation is obtained using E_3 voltage with poling in 3 directions. Torsion actuation is obtained using E_2 voltage with poling in 1 direction.

Here the δU terms for both the isotropic [20] and smart structure are obtained by using the variation of strain in the Hamilton's principle over the volume integral. The kinetic energy of the structure is modified due to change in mass and inertia by the addition of the smart layer, but virtual work done due to applied forces remain unchanged. The kinetic and strain energy terms of the isotropic beam are defined in Appendix C. The non-linear equations listed in Appendix C have been derived by Hodges and Dowell in 1974 [20] for elastic bending and torsion of twisted non-uniform rotor blades. Epps and Chandra [31] have validated the rotating frequencies predicted by the analysis with experimental data. Also Ganguli et al. [32] have validated the analysis with vibration data.

Following the above assumptions and the formulation for an isotropic beam [20], equations of motion for elastic bending and torsion of rotating beams with pretwist and surface bonded piezoceramic actuators are derived in this paper. Evaluating and deriving the new terms which arise due to surface bonding of the smart layer, yields

$$\begin{aligned}\frac{\delta U_{smart}}{m_0\Omega^2R^3} = \int_0^1 [&A_0(\delta u_e') + A_1(\theta_0' + \phi')\delta\phi' \\ &+ (-A_2\cos(\theta_0+\hat{\phi}) + A_3\sin(\theta_0+\hat{\phi}))(\delta v'' + w''\delta\hat{\phi}) \\ &+ (-A_2\sin(\theta_0+\hat{\phi}) - A_3\cos(\theta_0+\hat{\phi}))(\delta w'' + v''\delta\hat{\phi}) \\ &- (A_4\delta\hat{\phi}') - (A_5\delta\hat{\phi}'')]\,\mathrm{d}x,\end{aligned} \tag{8}$$

where A_0, A_1, A_2, A_3, A_4 and A_5 are the section properties due to piezoceramic actuation and are defined in Appendix B. The above derivation is generic for a beam undergoing displacements (axial, transverse bending, inplane bending and torsion), also it is generalized for axial, bending and torsional actuation.

2.2. Finite element discretization

A finite element discretization is done to solve the governing equations of motion to obtain the dynamic response of the system. After the finite element discretization the Hamilton's principle can be written as

$$\delta\Pi = \int_0^{2\pi} \sum_{i=1}^{N} (\delta U_i - \delta T_i - \delta W_i)\, \mathrm{d}\psi = 0. \tag{9}$$

The beam is discretized into N finite elements and each of these N beam finite elements have 15 degrees of freedom. The finite element discretization of the element used for the analysis is shown in Fig. 1. The degrees of freedom correspond to cubic variations in axial elastic, transverse bending and in-plane bending deflections. Elastic torsion has a quadratic variation. Element connectivity is established by continuity of slope and displacement for transverse and in-plane bending deflections whereas for elastic twist and axial deflection it is established by continuity of displacements. Such an element ensures linear variations of bending and torsion moments and quadratic variations of axial force within the elements. Substituting $\mathbf{u} = \mathbf{Hq}$ ($\mathbf{H}$ and $\mathbf{q}$ are given in Appendix D) in the Hamilton's principle we obtain

$$\int_0^{2\pi} \delta\mathbf{q}^{\mathrm{T}}(\mathbf{M}\ddot{\mathbf{q}}(\psi) + \mathbf{C}\dot{\mathbf{q}}(\psi) + \mathbf{K}\mathbf{q}(\psi) - \mathbf{F}(\mathbf{q}, \dot{\mathbf{q}}, \psi))\, \mathrm{d}\psi = 0. \tag{10}$$

The nodal displacements $\mathbf{q}$ are functions of time and all the non-linear terms are moved to the force vector. The spatial functionality has been removed by using finite element discretization and partial differential equations have been converted to ordinary differential equations. The finite element equations representing each rotor blade are transformed to normal mode space for efficient solution of blade response using the modal expansion. The displacements are expressed in

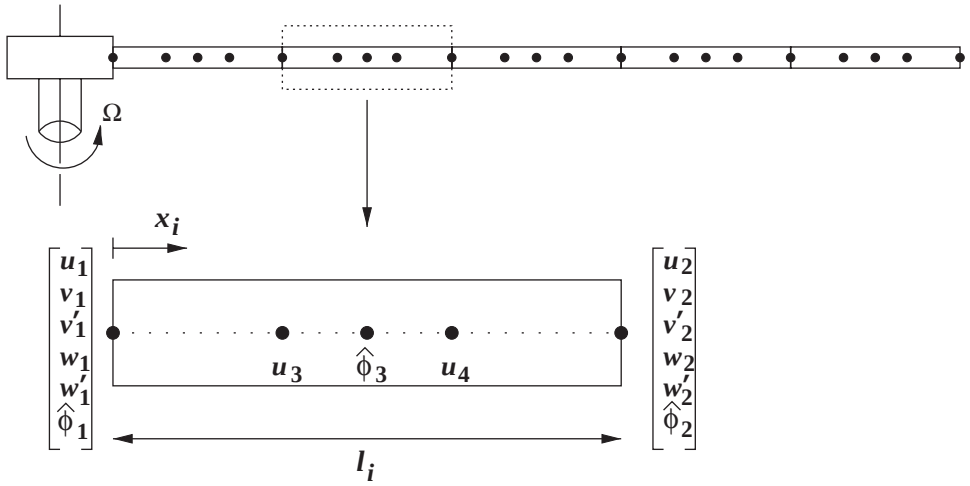

Fig. 1. The 15-DOF finite element model used for spatial discretization of the beam.

terms of normal modes as

$$\mathbf{q} = \mathbf{\Phi p}, \tag{11}$$

where $\mathbf{\Phi}$ is a matrix of the dimensions of blade degrees of freedom by number of modes selected for representation of blade response. Substitution of Eq. (11) in Eq. (10) leads to the normal mode equations of the form

$$\int_0^{2\pi} \delta\mathbf{p}^{\mathrm{T}}(\bar{\mathbf{M}}\ddot{\mathbf{p}}(\psi) + \bar{\mathbf{C}}\dot{\mathbf{p}}(\psi) + \bar{\mathbf{K}}\mathbf{p}(\psi) - \bar{\mathbf{F}}(\mathbf{p}, \dot{\mathbf{p}}, \psi)\,\mathrm{d}\psi = 0, \tag{12}$$

where the normal mode mass, stiffness, damping matrix and force vector are defined as $\bar{\mathbf{M}} = \mathbf{\Phi}^{\mathrm{T}}\mathbf{M}\mathbf{\Phi}$, $\bar{\mathbf{C}} = \mathbf{\Phi}^{\mathrm{T}}\mathbf{C}\mathbf{\Phi}$, $\bar{\mathbf{K}} = \mathbf{\Phi}^{\mathrm{T}}\mathbf{K}\mathbf{\Phi}$ and $\bar{\mathbf{F}} = \mathbf{\Phi}^{\mathrm{T}}\mathbf{F}$, respectively. Eq. (12) are non-linear ODEs but their dimensions are much reduced compared to the full finite element equations in Eq. (10). This is because only a few modes (typically 6–10) are needed to capture the dynamics of the problem. The mode shapes or eigen vectors can be obtained from undamped rotating frequency analysis of the blade, which is defined as $\bar{\mathbf{K}}_s\mathbf{\Phi} = \omega^2\mathbf{M}_s\mathbf{\Phi}$. Integrating Eq. (12) by parts we obtain

$$\int_0^{2\pi} \begin{Bmatrix} \delta\mathbf{p} \\ \delta\dot{\mathbf{p}} \end{Bmatrix} \begin{Bmatrix} \bar{\mathbf{F}} - \bar{\mathbf{C}}\dot{\mathbf{p}} - \bar{\mathbf{K}}\mathbf{p} \\ \bar{\mathbf{M}}\dot{\mathbf{p}} \end{Bmatrix} \mathrm{d}\psi = \begin{Bmatrix} \delta\mathbf{p} \\ \delta\dot{\mathbf{p}} \end{Bmatrix} \begin{Bmatrix} \bar{\mathbf{M}}\dot{\mathbf{p}} \\ 0 \end{Bmatrix} \Bigg|_0^{2\pi}. \tag{13}$$

Since the rotating beam is a periodic system with a time period of one revolution, we have $\dot{\mathbf{p}}(0) = \dot{\mathbf{p}}(2\pi)$. Imposing periodic boundary conditions on Eq. (13) results in the right hand side becoming zero and yields the following system of first order differential equations:

$$\int_0^{2\pi} \delta\mathbf{y}^{\mathrm{T}}\mathbf{Q}\,\mathrm{d}\psi = 0,$$

where

$$\mathbf{y} = \begin{Bmatrix} \mathbf{p} \\ \dot{\mathbf{p}} \end{Bmatrix} \quad \text{and} \quad \mathbf{Q} = \begin{Bmatrix} \bar{\mathbf{F}} - \bar{\mathbf{C}}\dot{\mathbf{p}} - \bar{\mathbf{K}}\mathbf{p} \\ \bar{\mathbf{M}}\dot{\mathbf{p}} \end{Bmatrix}. \tag{14}$$

The above equation is non-linear because $\bar{\mathbf{F}}$ contains non-linear terms. The non-linear, periodic, ordinary differential equations are then solved for blade steady response using the finite element in time by Newton–Raphson method. Discretizing Eq. (14) over N_t time elements around the circumference, (where $\psi_1 = 0$, $\psi_{N_t+1} = 2\pi$) and taking a first order Taylor's series expansion about the steady state value $\mathbf{y}_0 = [\mathbf{p}_0^{\mathrm{T}}\dot{\mathbf{p}}_0^{\mathrm{T}}]^{\mathrm{T}}$ yields algebraic equations.

$$\sum_{i=1}^{N_t} \int_{\psi_i}^{\psi_{i+1}} \delta\mathbf{y}_i^{\mathrm{T}}\mathbf{Q}_i(\mathbf{y}_0 + \Delta\mathbf{y})\,\mathrm{d}\psi = \sum_{i=1}^{N_t} \int_{\psi_i}^{\psi_{i+1}} \delta\mathbf{y}_i^{\mathrm{T}}[\mathbf{Q}_i(\mathbf{y}_0 + \mathbf{K}_{ti}(\mathbf{y}_0)\Delta\mathbf{y}]\,\mathrm{d}\psi = 0, \tag{15}$$

$$\mathbf{K}_{ti} = \begin{bmatrix} \frac{\partial\bar{\mathbf{F}}}{\partial\mathbf{p}} - \bar{\mathbf{K}} & \frac{\partial\bar{\mathbf{F}}}{\partial\dot{\mathbf{p}}} - \bar{\mathbf{C}} \\ 0 & \bar{\mathbf{M}} \end{bmatrix}_i. \tag{16}$$

Here $\mathbf{K}_{ti}$ is the tangential stiffness matrix for time element i and $\mathbf{Q}_i$ is the load vector. For the ith element, the time span is $\psi_{i+1} - \psi_i$ and there is continuity of the displacements between the time elements, also the modal displacement vector can be written as follows:

$$\mathbf{p}_i(\psi) = \mathbf{H}(s)\mathbf{r}_i, \tag{17}$$

where $\mathbf{H}(s)$ are the shape functions in time which are fifth order Lagrange polynomials (as defined in Appendix E) used for approximating the normal mode co-ordinate $\mathbf{p}$ within the elements and $\mathbf{r}$ is the temporal nodal co-ordinates vector. Eq. (17) expresses the time variation of the modal displacement vector. Substitution of Eq. (17) and its derivative in Eq. (15) results into the time discretized blade response.

$$\mathbf{Q}^G + \mathbf{K}_t^G \Delta\mathbf{r}^G = 0,$$

where

$$\mathbf{Q}^G = \sum_{i=1}^{N_t} \int_{\psi_i}^{\psi_{i+1}} \mathbf{H}^{\mathrm{T}} \mathbf{Q}_i \, \mathrm{d}\psi,$$

$$\mathbf{K}_t^G = \sum_{i=1}^{N_t} \int_{\psi_i}^{\psi_{i+1}} \mathbf{H}^{\mathrm{T}} \begin{bmatrix} \dfrac{\partial \bar{\mathbf{F}}}{\partial \mathbf{p}} - \bar{\mathbf{K}} & \dfrac{\partial \bar{\mathbf{F}}}{\partial \dot{\mathbf{p}}} - \bar{\mathbf{C}} \\ 0 & \bar{\mathbf{M}} \end{bmatrix}_i \mathrm{d}\psi,$$

$$\Delta\mathbf{r}^G = \sum_{i=1}^{N_t} \Delta\mathbf{r}_i. \tag{18}$$

Here $\mathbf{K}_t^G$ is the global tangential stiffness matrix and $\mathbf{Q}^G$ is the global load vector. Solving the above equations iteratively yields the blade steady response. The effect of the smart terms come in the stiffness matrix $\bar{\mathbf{K}}$ and the load vector $\bar{\mathbf{F}}$. The mass and damping are affected only by the material property(density) of the piezoceramic, and not by the actuation effect. All non-linear terms are moved to the load vector and **M, C** and **K** are linear. Other details regarding the solution procedure can be found in a recent paper by Ganguli [33].

2.3. Identification of smart structure terms

The governing equations derived in Eq. (8) (derived in the current study) and shown in Appendix C (derived by Hodges and Dowell [20]) contain a very large number of terms and are complicated to understand as they are derived for a generic cross-section beam with pretwist. For easy understanding of equations, few assumptions are made in the generic set of equations derived through variational principle (as shown in Eq. (8) and Appendix C). For the section shown in Fig. 2 (symmetric section) if $\theta_0 = 0$ and $\beta_p = 0$ then the following element stiffness, damping and

mass matrices are obtained. The linear and non-linear element force vectors are also shown for the same case.

$$\mathbf{K} = \frac{1}{2}\begin{bmatrix} \int_0^1 EAH_u'^{\mathrm{T}}H_u' \,\mathrm{d}s & 0 & 0 & 0 \\ 0 & \begin{matrix}\int_0^1 EI_z H'^{\mathrm{T}}H' \mathrm{d}s \\ + \int_0^1 F_A H'^{\mathrm{T}}H' \,\mathrm{d}s \\ - \int_0^1 mH^{\mathrm{T}}H \,\mathrm{d}s\end{matrix} & \int_0^1 A_4 H''^{\mathrm{T}}H' \,\mathrm{d}s & + \int_0^1 A_3 H''^{\mathrm{T}}H_{\hat{\phi}} \,\mathrm{d}s \\ 0 & \int_0^1 A_4 H''^{\mathrm{T}}H' \mathrm{d}s & \begin{matrix}\int_0^1 EI_y H'^{\mathrm{T}}H' \,\mathrm{d}s \\ + \int_0^1 F_A H'^{\mathrm{T}}H' \,\mathrm{d}s\end{matrix} & 0 \\ 0 & - \int_0^1 A_3 H''^{\mathrm{T}}H_{\hat{\phi}} \,\mathrm{d}s & 0 & \begin{matrix}\int_0^1 m(k_{m2}^2 - k_{m1}^2)H_{\hat{\phi}}^{\mathrm{T}}H_{\hat{\phi}} \,\mathrm{d}s \\ + \int_0^1 GJH_{\hat{\phi}}'^{\mathrm{T}}H_{\hat{\phi}}' \,\mathrm{d}s \\ + \int_0^1 A_1 H_{\hat{\phi}}'^{\mathrm{T}}H_{\hat{\phi}}' \,\mathrm{d}s\end{matrix} \end{bmatrix} \tag{19}$$

$$\mathbf{C} = \frac{1}{2}\begin{bmatrix} 0 & -\int_0^1 2mH_u^{\mathrm{T}}H_u \,\mathrm{d}s & 0 & 0 \\ \int_0^1 2mH_u^{\mathrm{T}}H_u \,\mathrm{d}s & 0 & 0 & 0 \\ 0 & 0 & 0 & 0 \\ 0 & 0 & 0 & 0 \end{bmatrix}. \tag{20}$$

$$\mathbf{M} = \frac{1}{2}\begin{bmatrix} \int_0^1 mH_u^{\mathrm{T}}H_u \,\mathrm{d}s & 0 & 0 & 0 \\ 0 & \int_0^1 mH^{\mathrm{T}}H \,\mathrm{d}s & 0 & 0 \\ 0 & 0 & \int_0^1 mH^{\mathrm{T}}H \,\mathrm{d}s & 0 \\ 0 & 0 & 0 & \int_0^1 mk_m^2 H_{\hat{\phi}}^{\mathrm{T}}H_{\hat{\phi}} \,\mathrm{d}s \end{bmatrix} \tag{21}$$

$$\mathbf{F}_L = \frac{1}{2}\begin{bmatrix} \int_0^1 mxH_u^{\mathrm{T}} \,\mathrm{d}s + \int_0^1 A_0 H_u^{\mathrm{T}} \,\mathrm{d}s \\ 0 \\ -\int_0^1 A_3 H''^{\mathrm{T}} \,\mathrm{d}s \\ +\int_0^1 A_4 H_{\hat{\phi}}'^{\mathrm{T}} \,\mathrm{d}s \end{bmatrix} \tag{22}$$

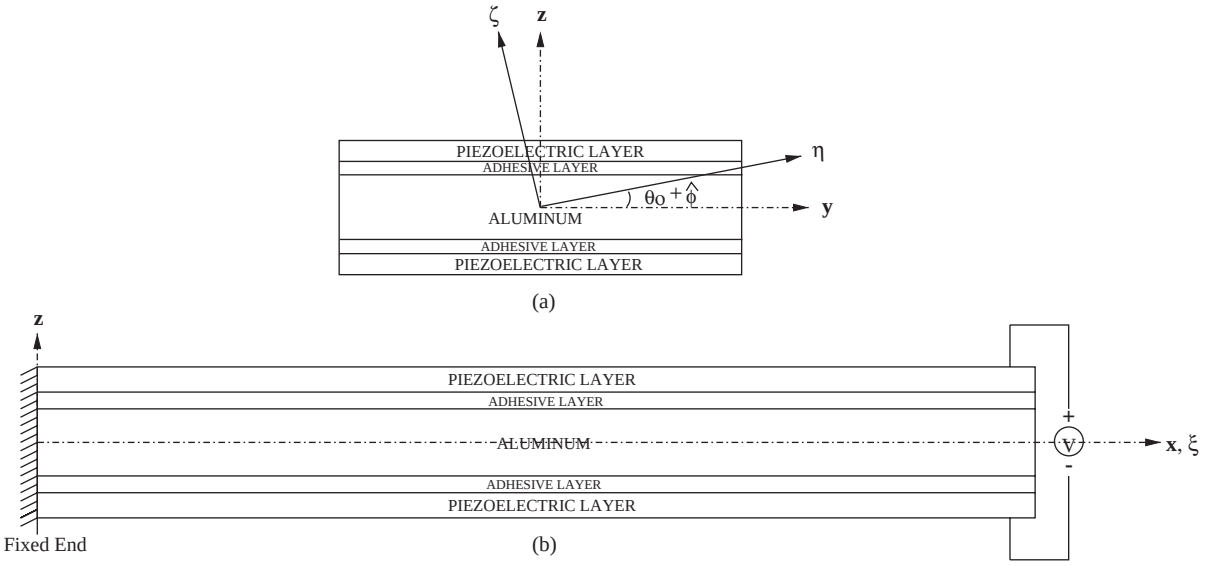

Fig. 2. (a) Cross-sectional view of the beam; (b) side view of the beam.

$$\mathbf{F}_{NL} = \frac{1}{2}\begin{bmatrix} -\int_0^1 EAk_A^2 \dfrac{\hat{\phi}^2}{2} H_u'^{\mathrm{T}}\,\mathrm{d}s \\ -\int_0^1 GJ\hat{\phi}'w'H''^{\mathrm{T}}\,\mathrm{d}s - \int_0^1 (EI_z - EI_y)w''\hat{\phi}H''^{\mathrm{T}}\,\mathrm{d}s + \int_0^1 A_1(\hat{\phi}w' + w'^2v'')H''^{\mathrm{T}}\,\mathrm{d}s \\ \quad + \int_0^1 2m\left[\int_0^x (v'\dot{v}' + w'\dot{w}')\,\mathrm{d}\xi\right]H^{\mathrm{T}}\,\mathrm{d}s - \int_0^1 (2v'\int_x^1 m\dot{v}\,\mathrm{d}\xi)H'^{\mathrm{T}}\,\mathrm{d}s \\ -\int_0^1 GJ\hat{\phi}'v''H'^{\mathrm{T}}\,\mathrm{d}s - \int_0^1 (2w'\int_x^1 m\dot{v}\,\mathrm{d}\xi)H'^{\mathrm{T}}\,\mathrm{d}s \\ -\int_0^1 (EI_z - EI_y)v''w''H_{\hat{\phi}}^{\mathrm{T}}\,\mathrm{d}s - \int_0^1 (EAk_A^2\hat{\phi}'u_e' + GJw'v'')H_{\hat{\phi}}'^{\mathrm{T}}\,\mathrm{d}s \\ \quad + \int_0^1 A_1w'v''H_{\hat{\phi}}'^{\mathrm{T}}\,\mathrm{d}s + \int_0^1 A_3w''\hat{\phi}H_{\hat{\phi}}^{\mathrm{T}}\,\mathrm{d}s \end{bmatrix}. \quad (23)$$

Here $F_A(x) = \int_1^x mx\,\mathrm{d}\xi$ is the centrifugal axial force due to the rotation. We observe that smart actuation terms cause inplane bending–transverse bending coupling and inplane–bending–torsion coupling through the stiffness terms. The mass matrix does not contain any specific smart structure terms. The damping matrix shows the presence of the antisymmetric Coriolis effect, but no influence of smart terms. The linear force vector shows the influence of smart actuation on the axial, transverse bending and torsion directions. Non-linear smart terms are present in the force vector for inplane bending and torsion forces. The above equations of motion can be used to identify terms that can be tailored by designing a beam cross-section to maximize the smart actuation effect and minimize the centrifugal stiffening effect.

3. Results and discussion

The model used for numerical results is a cantilevered aluminum beam with surface-mounted piezoceramic actuators as shown in Fig. 2. This model is similar to an experimental beam devised by Park et al. [34], allowing validation of the results with closed form solutions for a non-rotating bending beam. The cross-section of the beam is shown in Fig. 2(a). The cross-section can undergo twisting motion by an angle of $\theta_0 + \hat{\phi}$; where θ_0 is the applied control pitch and $\hat{\phi}$ is elastic twist. Thus it can move from the undeformed zy axes to the deformed $\eta\zeta$ axes about the axial co-ordinate x or ξ. The beam has a height of 1.28 mm, breadth of 50.8 mm, actuator thickness of 0.245 mm and adhesive thickness of 0.10 mm. The length of the beam is 406.4 mm. The adhesive layer has been considered here to incorporate the shear lag effects. The material properties considered for the results are given in Table 2. The results are obtained for a potential of 400 V in case of bending actuation and for 200 V in case of torsion actuation.

3.1. Bending actuation

For obtaining the bending actuation equal but opposite potentials are given to the top and the bottom piezo layers (bending motor concept)[35], which results into the expansion of one surface and contraction of other. As can be seen from Fig. 3, the poling direction is parallel to the direction of the potential. To bend the beam, a voltage of equal magnitude but opposite sign is applied to the top and bottom of actuators. Thus the beam bends to produce transverse bending deflection. For the non-rotating condition, a tip bending deflection of about 14 mm is obtained. This is slightly more than 3 percent of the beam length. Thus bending deflection obtained here matches with the closed form solution at the non-rotating level. Response for a rotating beam over a wide range of rotational speeds (0–100 Hz) is investigated. The transverse tip bending deflection and its variation with rotation speed is shown in Fig. 4. There is no other load on the beam except a bending moment due to bending actuation and the centrifugal loading due to rotation. It can be observed from Fig. 4 that there is a rapid fall in the bending deflection with increase in rotating speed. On studying the terms in Eqs. (19)–(23), it is noticed that the centrifugal stiffening effect ($\int_0^1 F_A H'^{\mathrm{T}} H' \, \mathrm{d}s$ in the stiffness matrix $\mathbf{K}$) counters the piezoceramic actuation force ($\int_0^1 A_3 H''^{\mathrm{T}} \, \mathrm{d}s$ in the linear force vector $\mathbf{F}_L$) and decreases the deflection which reduces to almost zero at higher rotation speeds. It therefore appears that bending actuation is useful for slowly rotating structures.

Table 2
Mechanical properties considered for simulation

PZT-5H	Adhesive	Aluminum	Units
$E = 62 \times 10^3$	$E = 3.068 \times 10^3$	$E = 68.94 \times 10^3$	MPa
$v = 0.3$	$v = 0.3485$	$v = 0.3$	—
$\rho = 7500$	$\rho = 1000$	$\rho = 2700$	kg/m^3
$d_{31} = 274 \times 10^{-09}$	—	—	mm/V
$d_{15} = 740 \times 10^{-09}$	—	—	mm/V

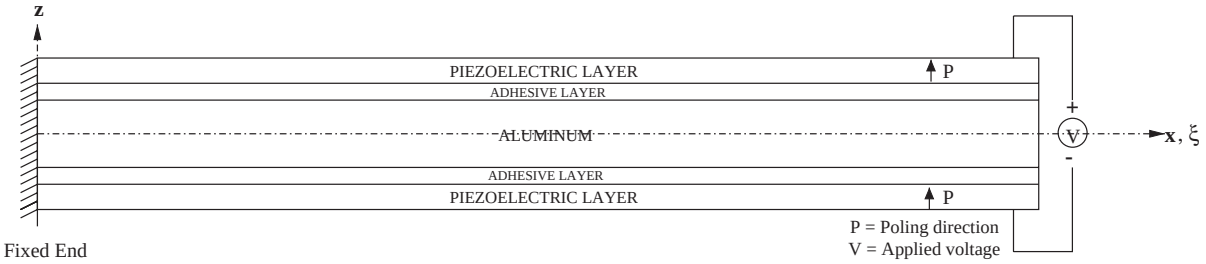

Fig. 3. Schematic of bending actuation (poling direction is parallel to applied voltage).

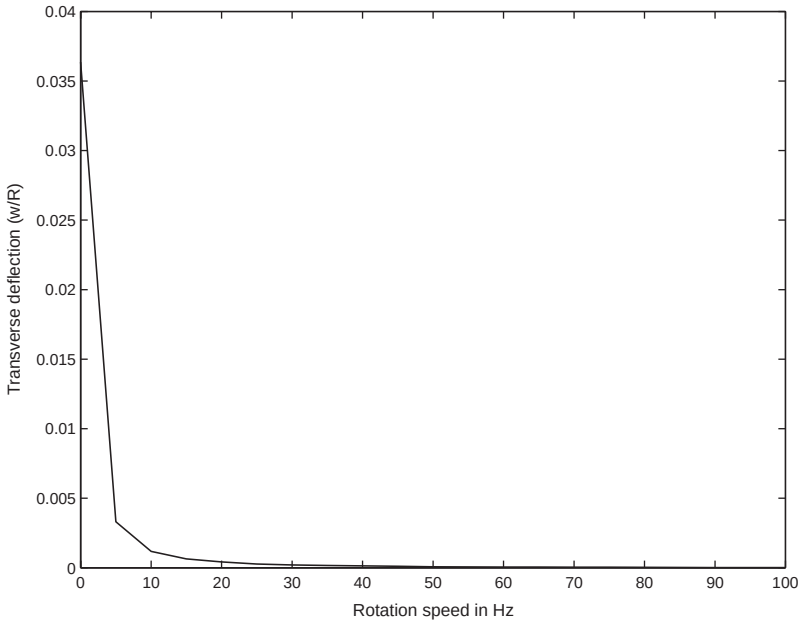

Fig. 4. Transverse tip bending deflection for beam with bending actuation and increasing rotation speed.

3.2. Torsional actuation

Torsional actuation is obtained by exploiting the parallel shear motor concept [35]. Poling direction in the case of torsional or shear actuation is perpendicular to the application of potential as shown in Fig. 5. This differs from the extension and bending actuators where the poling direction is always parallel to the application of the potential, neglecting the inherent shear effects. Hence, the piezoelectric constant d_{15} is not highlighted. Recently a few d_{15} based torsional actuators [26–28] have been proposed. These have been suggested for obtaining large torque and angular displacement. The main reasons [18] for using the shear actuator mechanism are: (1) d_{15} based torsional actuators produce large angular displacement and torque; (2) the performance of shear actuators is less dependent on structure's stiffness; (3) less problems of actuator debonding at its extremities; (4) d_{15} has a higher value than d_{31} and d_{33}.

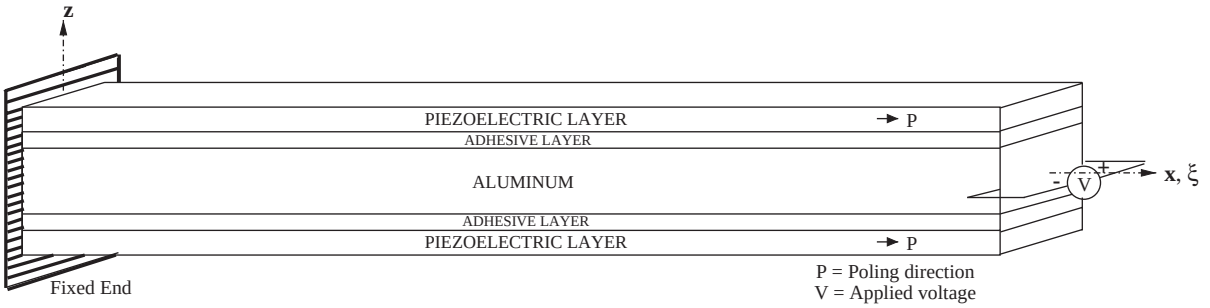

Fig. 5. Schematic of shear actuation (poling direction is perpendicular to applied voltage).

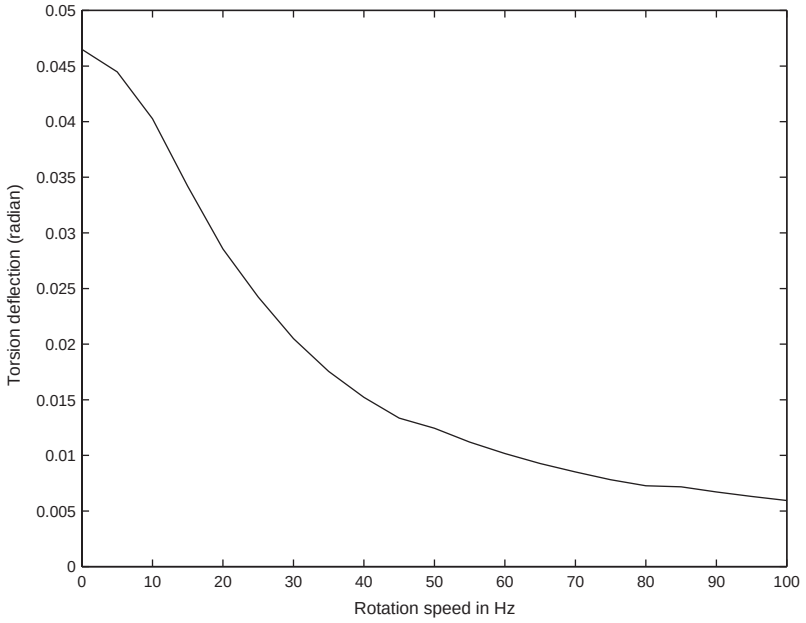

Fig. 6. Torsion deflection at tip for beam with torsion actuation and increasing rotating speed.

The principal torsional actuation term is $\int_0^1 A_4 H_{\hat{\phi}}^{\mathrm{T}} \, \mathrm{d}s$ in the linear load vector. The stiffening terms are $\int_0^1 GJ H_{\hat{\phi}}^{\prime\mathrm{T}} H_{\hat{\phi}}^{\prime} \, \mathrm{d}s$ coming from the structural stiffness and $\int_0^1 m\Omega^2(k_{m2}^2 - k_{m1}^2) H_{\hat{\phi}}^{\mathrm{T}} H_{\hat{\phi}} \, \mathrm{d}s$ coming from the rotational effect. According to the requirements of the problem, the term A_4 and GJ involved in torsion actuation and structural stiffening respectively, can be tailored so as to yield maximum torsion actuation.

In Fig. 6, torsional response is plotted with increasing rotation speed. There is no other load on the beam except the smart couple (shear actuation) and the propeller moment caused by centrifugal force. This is compared with the zero loading situation. In the case of torsion a twist of 2.66° is obtained for the non-rotating case, which decreases as the rotation speed increases. At rotation speed as high as 100 Hz, a twist of around 0.35° is obtained. However, the decrease in twist with rotation speed is much less when compared to the decrease in bending (observed in

previous section). This is because the centrifugal stiffening of the torsion mode is less compared to that of the transverse bending mode. It can be seen from Eq. (22) that the term leading to the centrifugal stiffening in the torsion direction is $\int_0^1 m\Omega^2(k_{m2}^2 - k_{m1}^2)H_{\hat{\phi}}^{\mathrm{T}} H_{\hat{\phi}}\,\mathrm{d}s$ whereas in the bending direction is $\int_0^1 F_A H_u'^{\mathrm{T}} H_u'\,\mathrm{d}s$. The latter term is larger in value. Thus it can be said that in case of torsion response, there remains enough twist to enable active control of vibration reduction even at high rotation speeds. Whereas in case of transverse bending, the centrifugal stiffening effect almost nullifies the effect of piezoceramic actuation at high rotation speeds. Shear based piezoceramic actuation using the d_{15} term appears useful for torsion actuation of rotating beams.

3.3. Torsion actuation with sinusoidal loads

The above results were obtained with the only loads acting on the beam being those due to rotation and actuation. Also the deflections were only due to smart actuation and were too small to activate the non-linear terms, which are motion dependent. To examine the effects of the non-linear terms and time varying loading, a sinusoidal tip load is given to a beam rotating at 100 Hz. Torsional response (torsion actuation) considering non-linear and linear effects is shown in Fig. 7. The linear effects are obtained by suppressing the non-linear terms in the computer program used for getting the results. Results for the linear and non-linear cases are obtained for (1) no smart actuation and (2) with smart actuation. There is considerable change in the response pattern for linear and non-linear case. The smart loading also follows the same pattern, giving it a shift by some magnitude, showing that with a smart loading a valuable amount of change in response can be obtained.

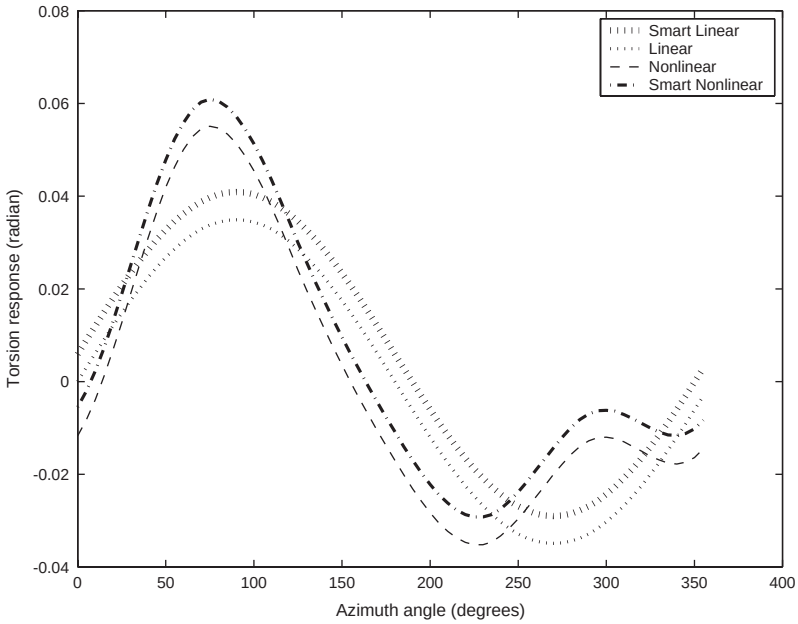

Fig. 7. Effect of non-linear terms on tip torsion response under tip sinusoidal load and rotation speed of 100 Hz with and without smart torsion actuation.

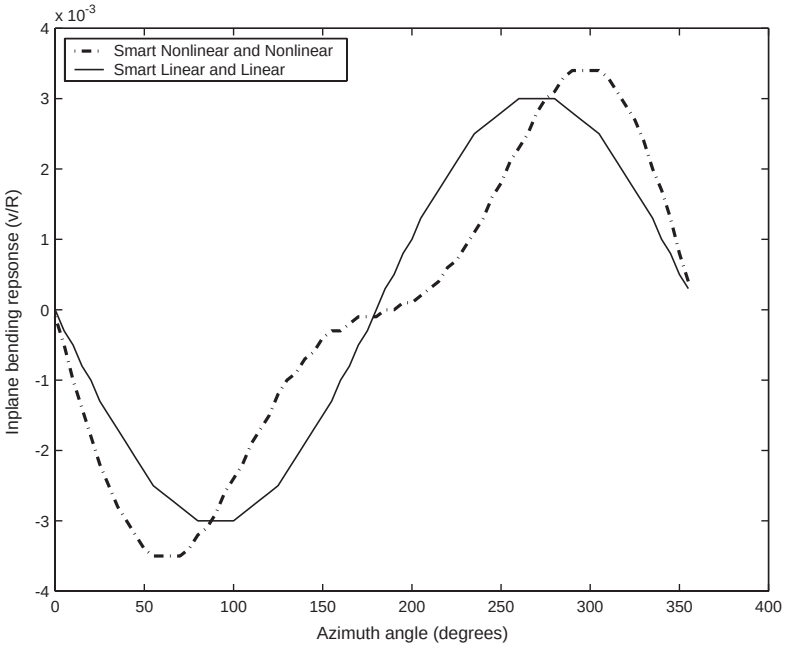

Fig. 8. Effect of non-linear terms on tip in-plane bending response under tip sinusoidal load and rotation speed of 100 Hz with and without smart torsion actuation.

The non-linear effect in the case of inplane and transverse bending response (torsion actuation) can be seen in Figs. 8 and 9, respectively. Here the magnitude of difference between the non-linear and the linear cases is smaller when compared to torsion. The importance of including non-linear terms in the analysis is clear, especially for accurate prediction of torsion response.

3.4. Bending actuation with sinusoidal loads

A similar case as described above is then examined with the smart couple in the form of a bending actuation and the beam rotating at 10 Hz. The non-linear and smart effect in the case of transverse bending, inplane and torsion response are shown in Figs. 10, 11 and 12, respectively. In the case of inplane and transverse bending (bending actuation), the effect of non-linear terms is smaller than for torsion.

It can be noted from the figures that the d_{15} type actuation (Fig. 7) has a greater impact on the torsion response of the rotating beam than the d_{31} type actuation (Fig. 12). Notable difference can be seen between baseline and smart case for both linear and non-linear analysis. Thus it can be said that the utility of d_{15} based piezoceramic actuators can be exploited for applications in which torsion mode of response is of importance.

3.5. Torsion actuation with pretwist

Rotating systems create accelerations arising from the elastic structural deformations, Coriolis and centripetal forces. The complexity increases further when initial pretwist is also included in a

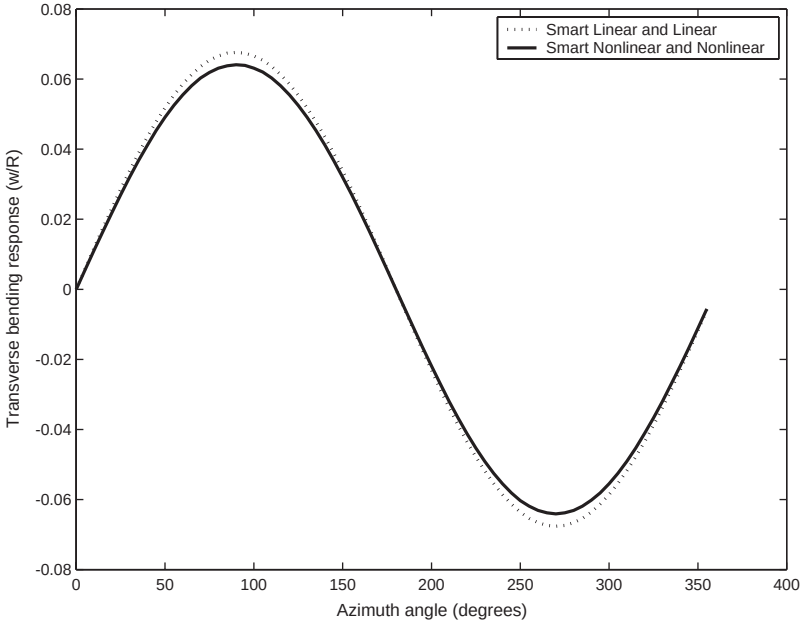

Fig. 9. Effect of non-linear terms on tip transverse bending response under tip sinusoidal load and rotation speed of 100 Hz with and without smart torsion actuation.

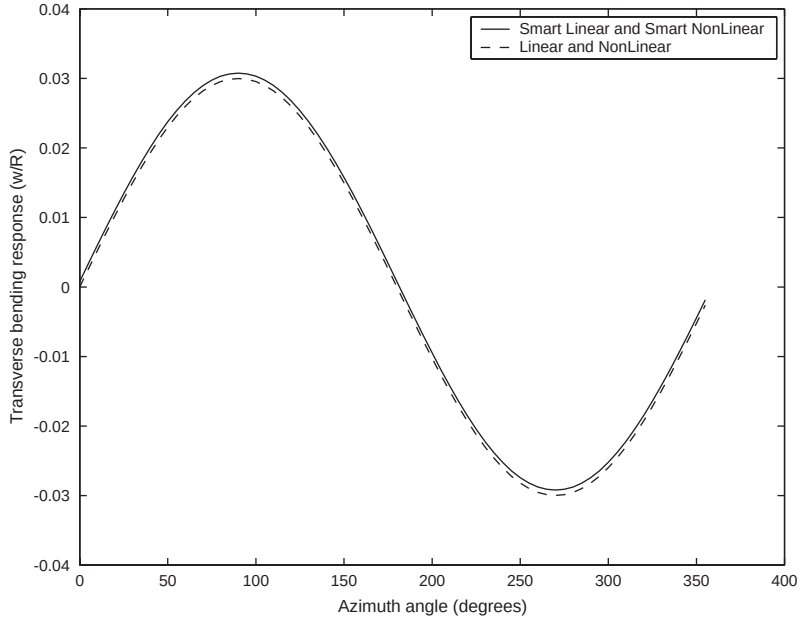

Fig. 10. Effect of non-linear terms on tip transverse bending response under tip sinusoidal load and rotation speed of 10 Hz with and without smart bending actuation.

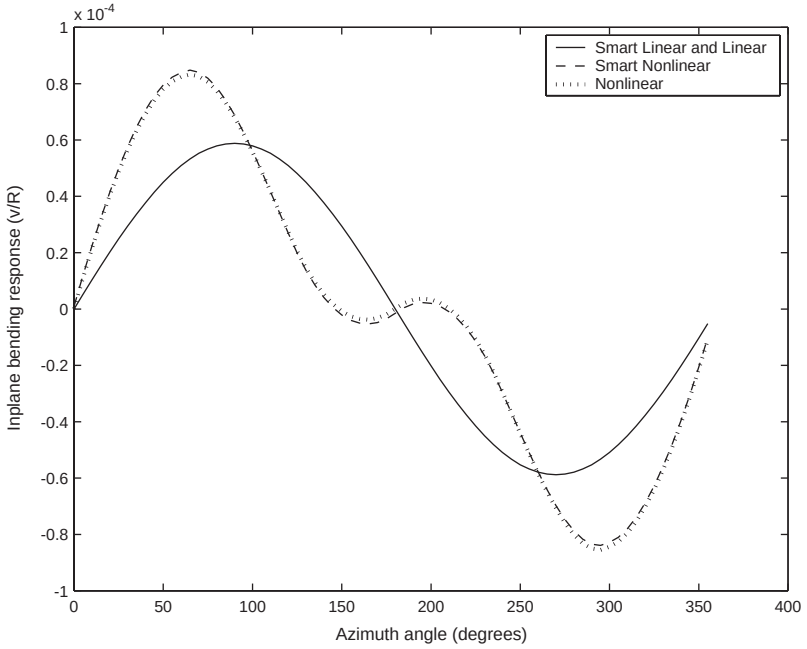

Fig. 11. Effect of non-linear terms on tip inplane bending response under tip sinusoidal load and rotation speed of 10 Hz with and without smart bending actuation.

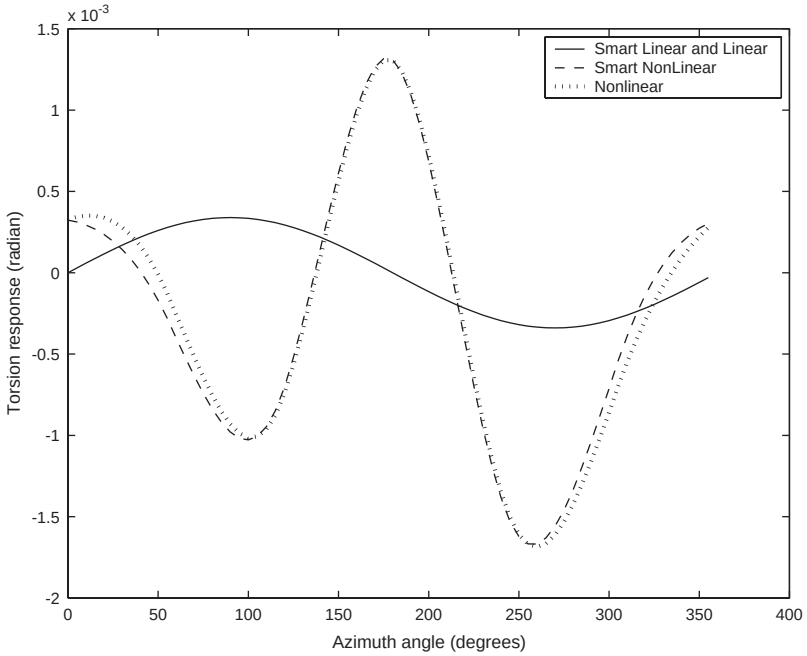

Fig. 12. Effect of non-linear terms on tip torsion response under tip sinusoidal load and rotation speed of 10 Hz with and without smart bending actuation.

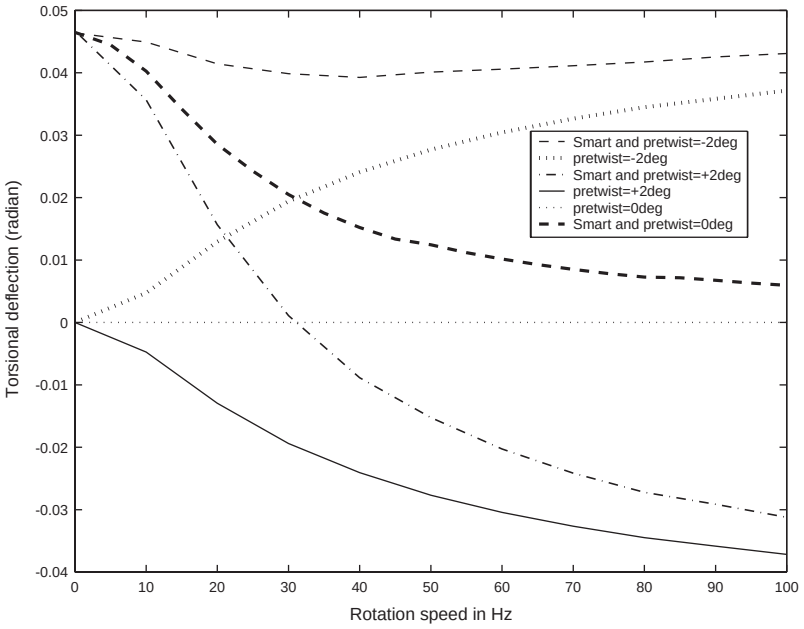

Fig. 13. Effect of pretwist and smart torsion actuation tip torsion deflection with increasing rotation speed.

beam as additional couplings are introduced due to the pretwist which can affect the beam response to static and dynamic loads [36–38]. In this paper, an example has been taken of a beam which is pretwisted by (a) 2° and (b) -2°. Linear pretwist is considered for these cases. A torsional smart moment is then applied on such a beam through the shear mode as discussed in Section 3.2. It can be noted from Fig. 13 that at a pretwist of $\pm 2^\circ$, the torsional deflection varies approximately from 0° to 2.29° at a rotation speed of 0–100 Hz. But when a smart torsional moment is applied the trend followed by the torsional deflection changes. There is a difference in the tip torsional response of about 2.69° at $\Omega = 0$, which reduces to about 0.17° at $\Omega = 100$ Hz.

The effect of the piezoceramic actuation is to increase the torsion deflection of the beam. The increase is maximum in the non-rotating condition and becomes less as rotation speed increases. It can be observed from this example of $\pm 2^\circ$ pretwist that combinations of smart actuation and pretwist can be worked out to obtain a desired torsion deflection over a range of rotation speeds. Similar attempts were made on applying bending actuation to a pretwisted beam but the results obtained showed very little change and hence have not been presented here. Thus it can be said that torsion actuation proves to be a better alternative in this case.

4. Conclusions

Governing equations for a beam with piezoceramic actuation and undergoing transverse bending, inplane bending, axial and torsion displacements are derived. Non-linear terms accounting for moderate deflections are retained in the analysis. The blade equations are

discretized and solved in the spatial and time domain using the finite element method. Numerical results are obtained over a range of rotation speeds for (1) smart actuation only, (2) smart actuation and sinusoidal tip load and (3) smart actuation with pretwist. The following conclusions are drawn from this study:

(1) Results show that rotation greatly reduces the transverse bending caused by piezoceramic actuation due to centrifugal stiffening of the blade. However, the reduction in torsion response is much less and there remains enough twist actuation for active control of vibration reduction and other applications even at rotation speeds as high as 100 Hz. Bending actuation may be feasible for slowly rotating structures such as wind turbine rotors.
(2) The bending actuation mechanism (d_{31} effect) produces a bending couple which controls the transverse bending response of the structure and the shear actuation mechanism (d_{15} effect) produces the torsional couple which can control the torsion response of the structure. Shear based piezoceramic actuation using the d_{15} term appears to be useful for torsional actuation of rotating beams.
(3) The equations of motion derived in this study can be used to identify terms that can be tailored by designing a cross-section to maximize the smart actuation effect and minimize the centrifugal stiffening effect.
(4) It is possible to combine smart actuation and pretwist to get a desired torsional deflection over a range of rotation speeds.
(5) The non-linear effects are important for accurate torsional response prediction for a smart rotating beam.

Appendix A. Nomenclature

$\mathbf{C}$	finite element damping matrix
e_g	chordwise offset of blade center-of-mass ahead of elastic axis
E	Young's modulus
EI_y	transverse bending stiffness
EI_z	in-plane bending stiffness
$\mathbf{F}$	finite element force vector
$\mathbf{F}_L$	finite element linear force vector
$\mathbf{F}_{NL}$	finite element non-linear force vector
G	shear modulus
GJ	torsion stiffness
k_A	radius of gyration of the blade cross-section
k_{m1}	blade cross-sectional mass radius of gyration in the transverse direction
k_{m2}	blade cross-sectional mass radius of gyration in the in-plane direction
$\mathbf{K}$	finite element stiffness matrix
$\bar{\mathbf{K}}_s$	global structural stiffness matrix
l_i	length of the ith beam element
m_0	mass per unit length of blade
$\mathbf{M}$	finite element mass matrix

$\bar{\mathbf{M}}_s$	global structural mass matrix
N	number of spatial finite elements
N_t	number of time elements for one rotor revolution
$\mathbf{p}$	modal displacement vector
$\mathbf{P}$	poling direction
$\mathbf{q}$	global displacement vector
$\mathbf{Q}$	generalized load vector for response analysis
$\mathbf{r}$	temporal nodal displacement vector for time element
R	rotor radius
T	kinetic energy
u	axial deflection of blade
u_e	elastic axial deflection
U	strain energy
U_S	smart structure contribution to strain energy
v	in-plane bending deflection of blade
w	transverse bending deflection of blade
W	virtual work
x	longitudinal direction
y	lateral direction
z	vertical direction
β_p	blade precone
γ	shear strain
δ	variation
$\varepsilon_{xx}, \varepsilon_{\eta\eta}, \varepsilon_{\zeta\zeta}$	normal strains
$\varepsilon_{x\eta}, \varepsilon_{\eta\zeta}, \varepsilon_{x\zeta}$	shear strains
ζ, η, ξ	rotating deformed blade coordinate system
θ_0	rigid pitch angle due to control pitch and pretwist
λ_T	warping function
v	Poisson ratio
ρ_s	density
$\sigma_{xx}, \sigma_{\eta\eta}, \sigma_{\zeta\zeta}$	normal stresses
$\tau_{x\eta}, \tau_{\eta\zeta}, \tau_{x\zeta}$	shear stresses
ϕ	elastic twist
ψ	azimuth angle, time
Ω	rotation speed, scalar quantity

Appendix B. Section properties

$$A_0 = \int_\eta \int_\zeta EP \, \mathrm{d}\eta \, \mathrm{d}\zeta,$$

$$A_1 = \int_\eta \int_\zeta EP(\eta^2 + \zeta^2) \, \mathrm{d}\eta \, \mathrm{d}\zeta,$$

$$A_2 = \int_\eta \int_\zeta (EP\eta)\,\mathrm{d}\eta\,\mathrm{d}\zeta,$$

$$A_3 = \int_\eta \int_\zeta (EP\zeta)\,\mathrm{d}\eta\,\mathrm{d}\zeta,$$

$$A_4 = \int_\eta \int_\zeta (2G_{piezo}P_1\zeta)\,\mathrm{d}\eta\,\mathrm{d}\zeta,$$

$$A_5 = \int_\eta \int_\zeta (EP\eta\zeta)\,\mathrm{d}\eta\,\mathrm{d}\zeta,$$

$$EI_y = \int_\eta \int_\zeta E\zeta^2\,\mathrm{d}\eta\,\mathrm{d}\zeta,$$

$$EI_z = \int_\eta \int_\zeta E\eta^2\,\mathrm{d}\eta\,\mathrm{d}\zeta,$$

$$EA = \int_\eta \int_\zeta E\,\mathrm{d}\eta\,\mathrm{d}\zeta,$$

$$GJ = \int_\eta \int_\zeta G(\hat{\eta}^2 + \hat{\zeta}^2)\,\mathrm{d}\eta\,\mathrm{d}\zeta,$$

$$EB_1 = \int_\eta \int_\zeta E(\eta^2 + \zeta^2)\,\mathrm{d}\eta\,\mathrm{d}\zeta,$$

$$EC_1 = \int_\eta \int_\zeta E\lambda_T^2\,\mathrm{d}\eta\,\mathrm{d}\zeta,$$

$$EAe_A = \int_\eta \int_\zeta E\eta\,\mathrm{d}\eta\,\mathrm{d}\zeta,$$

$$EAk_A^2 = \int_\eta \int_\zeta E(\eta^2 + \zeta^2)\,\mathrm{d}\eta\,\mathrm{d}\zeta,$$

$$EB_2 = \int_\eta \int_\zeta E\eta(\eta^2 + \zeta^2)\,\mathrm{d}\eta\,\mathrm{d}\zeta,$$

$$EC_2 = \int_\eta \int_\zeta E\zeta\lambda_T\,\mathrm{d}\eta\,\mathrm{d}\zeta,$$

where P and P_1 depend on piezoelectric properties and are given as $P = d_{31}E_3$ and $P_1 = d_{15}E_2$. However, A_0, A_1, A_2, A_3, A_4, A_5 depend on piezoelectric and section properties.

Appendix C. Kinetic and strain energy terms

$$\frac{\delta U_{iso}}{m_0\Omega^2R^3} = \int_0^1 (U_{u'_e}\delta u'_e + U_{v'}\delta v' + U_{w'}\delta w' + U_{v''}\delta v'' + U_{w''}\delta w'' + U_{\hat{\phi}}\delta\hat{\phi} + U_{\hat{\phi}'}\delta\hat{\phi}' + U_{\hat{\phi}''}\delta\hat{\phi}'')\,\mathrm{d}x$$

where

$$U_{u'_e} = EA\left[u'_e + k_A^2\theta'_0(\hat{\phi}' + w'v'') + k_A^2\frac{\hat{\phi}'^2}{2}\right] - EAe_A[v''(\cos\theta_0 - \hat{\phi}\sin\theta_0) + w''(\sin\theta_0 + \hat{\phi}\cos\theta_0)],$$

$$U_{v''} = v''(EI_z\cos^2\theta_0 + EI_y\sin^2\theta_0) + w''(EI_z - EI_y)\cos\theta_0\sin\theta_0 - EAe_Au'_e(\cos\theta_0 - \hat{\phi}\sin\theta_0) - \hat{\phi}'EB_2\theta'_0\cos\theta_0 + w''\hat{\phi}(EI_z - EI_y)\cos 2\theta_0 - v''\hat{\phi}(EI_z - EI_y)\sin 2\theta_0 + (GJ + EB_1\theta'^2_0)\hat{\phi}'w' + EAk_A^2\theta'_0w'u'_e,$$

$$U_{w'} = (GJ + EB_1\theta'^2_0)\hat{\phi}'v'' + EAk_A^2\theta'_0v''u'_e,$$

$$U_{w''} = w''(EI_y\cos^2\theta_0 + EI_z\sin^2\theta_0) + v''(EI_z - EI_y)\cos\theta_0\sin\theta_0 - EAe_Au'_e(\sin\theta_0 + \hat{\phi}\cos\theta_0) - \hat{\phi}'EB_2\theta'_0\sin\theta_0 + w''\hat{\phi}(EI_z - EI_y)\sin 2\theta_0 + v''\hat{\phi}(EI_z - EI_y)\cos 2\theta_0,$$

$$U_{\hat{\phi}} = w''^2(EI_z - EI_y)\sin\theta_0\cos\theta_0 + v''w''(EI_z - EI_y)\cos 2\theta_0 - v''^2(EI_z - EI_y)\sin\theta_0\cos\theta_0,$$

$$U_{\hat{\phi}'} = GJ(\hat{\phi}' + w'v'') + EB_1\theta'^2_0\hat{\phi}' + EAk_A^2(\theta'_0 + \hat{\phi}')u'_e - EB_2\theta'_0(v''\cos\theta_0 + w''\sin\theta_0),$$

$$U_{\hat{\phi}''} = EC_1\hat{\phi}'' + EC_2(w''\cos\theta_0 - v''\sin\theta_0),$$

$$\frac{\delta T}{m_0\Omega^2R^3} = \int_0^1 m(T_{u_e}\delta u_e + T_v\delta v + T_w\delta w + T_{v'}\delta v' + T_{w'}\delta w' + T_\phi\delta\phi + T_F)\,\mathrm{d}x,$$

where

$$T_{u_e} = x + u_e + 2\dot{v} - \ddot{u}_e,$$

$$T_v = e_g(\cos\theta_0 + \ddot{\theta}_0\sin\theta_0) + v - \hat{\phi}e_g\sin\theta_0 + 2\dot{w}\beta_p + 2\dot{v}'e_g\cos\theta_0 + 2\dot{w}'e_g\sin\theta_0 - \ddot{v} + \hat{\ddot{\phi}}e_g\sin\theta_0 - 2\dot{u}_e + 2\int_0^x(v'\dot{v}' + w'\dot{w}')\,\mathrm{d}\xi,$$

$$T_{v'} = -e_g(x\cos\theta_0 - \hat{\phi}x\sin\theta_0 + 2\dot{v}\cos\theta_0),$$

$$T_w = -x\beta_p - \ddot{\theta}_0e_g\cos\theta_0 - 2\dot{v}\beta_p - \ddot{w} - \hat{\ddot{\phi}}e_g\cos\theta_0,$$

$$T_{w'} = -e_g(x\sin\theta_0 + \hat{\phi}x\cos\theta_0 + 2\dot{v}\sin\theta_0),$$

$$T_{\hat{\phi}} = -k_m^2\hat{\ddot{\phi}} - (k_{m2}^2 - k_{m1}^2)\cos\theta_0\sin\theta_0 - x\beta_pe_g\cos\theta_0 - ve_g\sin\theta_0 + v'xe_g\sin\theta_0 - w'xe_g\cos\theta_0 + \ddot{v}e_g\sin\theta_0 - \hat{\phi}(k_{m2}^2 - k_{m1}^2)\cos 2\theta_0 - \ddot{w}e_g\cos\theta_0 - k_m^2\ddot{\theta}_0,$$

$$T_F = -(x + 2\dot{v})\int_0^x(v'\delta v' + w'\delta w')\,\mathrm{d}\xi.$$

The radial shortening term T_F can be written as

$$-\int_0^1 mT_F\,\mathrm{d}x = \int_0^1 m(x+2\dot{v})\left[\int_0^x (v'\delta v' + w'\delta w')\,\mathrm{d}\xi\right]\mathrm{d}x.$$

Integrating by parts leads to a more convenient form

$$-\int_0^1 mT_F\,\mathrm{d}x = \int_0^1 F_A(v'\delta v' + w'\delta w')\,\mathrm{d}x + \int_0^1 (v'\delta v' + w'\delta w')\left[\int_x^1 2m\dot{v}\,\mathrm{d}\xi\right]\mathrm{d}x,$$

where the centrifugal force F_A is defined as

$$F_A(x) = \int_1^x mx\,\mathrm{d}\xi$$

which gives the "centrifugal stiffening" effect on the transverse bending and in-plane bending equations. In this case the blade sectional integral are defined as

$$m = \int\int_A \rho_s\,\mathrm{d}\eta\,\mathrm{d}\zeta,$$

$$me_g = \int\int_A \rho_s\eta\,\mathrm{d}\eta\,\mathrm{d}\zeta,$$

$$mk_{m1}^2 = \int\int_A \rho_s\zeta^2\,\mathrm{d}\eta\,\mathrm{d}\zeta,$$

$$mk_{m2}^2 = \int\int_A \rho_s\eta^2\,\mathrm{d}\eta\,\mathrm{d}\zeta,$$

$$mk_m^2 = mk_{m1}^2 + mk_{m2}^2.$$

Appendix D. Shape functions for space

$$u(s) = \begin{Bmatrix} u(s) \\ v(s) \\ w(s) \\ \hat{\phi}(s) \end{Bmatrix} = \begin{bmatrix} H_u & 0 & 0 & 0 \\ 0 & H & 0 & 0 \\ 0 & 0 & H & 0 \\ 0 & 0 & 0 & H_{\hat{\phi}} \end{bmatrix} q_i,$$

$$H_u^{\mathrm{T}} = \begin{Bmatrix} H_{u1} \\ H_{u2} \\ H_{u3} \\ H_{u4} \end{Bmatrix} = \begin{Bmatrix} -4.5s^3 + 9s^2 - 5.5s + 1 \\ 13.5s^3 - 22.5s^2 + 9s \\ -13.5s^3 + 18s^2 - 4.5s \\ 4.5s^3 - 4.5s^2 + s \end{Bmatrix},$$

$$H^{\mathrm{T}} = \begin{Bmatrix} H_1 \\ H_2 \\ H_3 \\ H_4 \end{Bmatrix} = \begin{Bmatrix} 2s^3 - 3s^2 + 1 \\ l_i(s^3 - 2s^2 + s) \\ -2s^3 + 3s^2 \\ l_i(s^3 - s^2) \end{Bmatrix},$$

$$H_{\hat{\phi}}^{\mathrm{T}} = \begin{Bmatrix} H_{\hat{\phi}1} \\ H_{\hat{\phi}2} \\ H_{\hat{\phi}3} \end{Bmatrix} = \begin{Bmatrix} 2s^2 - 3s + 1 \\ -4s^2 + 4s \\ 2s^2 - s \end{Bmatrix},$$

where $q_i^{\mathrm{T}} = [u_1, u_2, u_3, u_4, v_1, v_1', v_2, v_2', w_1, w_1', w_2, w_2', \hat{\phi}_1, \hat{\phi}_2, \hat{\phi}_3]$ and $s = \frac{x_i}{l_i}$.

Appendix E. Shape functions for time

$$\begin{Bmatrix} H_{t1}(s) \\ H_{t2}(s) \\ H_{t3}(s) \\ H_{t4}(s) \\ H_{t5}(s) \\ H_{t6}(s) \end{Bmatrix} = \begin{Bmatrix} \frac{1}{24}(-625s^5 + 1875s^4 - 2125s^3 + 1125s^2 - 274s + 24) \\ \frac{1}{24}(3125s^5 - 8750s^4 + 8875s^3 - 3850s^2 + 600s) \\ \frac{1}{12}(-3125s^5 + 8125s^4 - 7375s^3 + 2675s^2 - 300s) \\ \frac{1}{12}(3125s^5 - 7500s^4 + 6125s^3 - 1950s^2 + 200s) \\ \frac{1}{24}(-3125s^5 + 6875s^4 - 5125s^3 + 1525s^2 - 150s) \\ \frac{1}{24}(625s^5 - 1250s^4 + 875s^3 - 250s^2 + 24s) \end{Bmatrix}.$$

References

[1] E. Crawley, Intelligent structures for aerospace: a technology overview and assessment, American Institute of Aeronautics and Astronautics Journal 32 (1994) 1689–1699.

[2] V. Giurgiutiu, Review of smart-materials actuation solutions for aeroelastic and vibration control, Journal of Intelligent Material Systems and Structures 11 (2000) 525–543.

[3] I. Chopra, Status of application of smart structures technology to rotorcraft systems, Journal of American Helicopter Society 45 (2000) 228–252.

[4] C. Wang, K. Ang, A. Ajit, Shape control of laminated cantilevered beams with piezoceramic actuators, Journal of Intelligent Material Systems and Structures 10 (1999) 164–175.

[5] D. Robbins, J. Reddy, Analysis of piezoelectrically actuated beams using a layer-wise displacement theory, Journal of Computers and Structures 41 (1990) 265–279.

[6] N. Lobontiu, M. Goldfarb, E. Garcia, Achieving maximum tip displacement during resonant excitation of piezoelectrically actuated beams, Journal of Intelligent Material Systems and Structures 10 (1999) 900–913.

[7] D. Huang, B. Sun, Approximate analytical solutions of smart composite mindlin beams, Journal of Sound and Vibration 244 (2001) 379–394.

[8] M. Friswell, On the design of modal actuators and sensors, Journal of Sound and Vibration 241 (2001) 361–372.

[9] D. Sun, L. Tong, Sensor/actuator equations for curved piezoelectric fibers and vibration control of composite beams using fiber modal actuators/sensors, Journal of Sound and Vibration 241 (2001) 297–314.

[10] L. Librescu, L. Meirovitch, S. Na, Control of cantilever vibration via structural tailoring and adaptive materials, American Institute of Aeronautics and Astronautics Journal 35 (1997) 1309–1315.
[11] P. Chen, I. Chopra, Hover testing of smart rotor with induced-strain actuation of blade twist, American Institute of Aeronautics and Astronautics Journal 35 (1997) 6–16.
[12] S. Rao, R. Gupta, Finite element vibration analysis of rotating Timoshenko beams, Journal of Sound and Vibration 242 (2001) 103–124.
[13] S. Lin, K. Hsio, Vibration analysis of a rotating Timoshenko beam, Journal of Sound and Vibration 240 (2001) 303–322.
[14] D. Diker, Vibration control of a rotating Euler–Bernoulli beam, Journal of Sound and Vibration 232 (2000) 541–551.
[15] J. Chung, H. Yoo, Dynamic analysis of a rotating cantilever beam by using the finite element method, Journal of Sound and Vibration 249 (2002) 147–164.
[16] D. Hodges, Y. Chung, X. Shang, Discrete transfer matrix method for non-uniform rotating beams, Journal of Sound and Vibration 240 (1994) 276–283.
[17] A. Chattopadhyay, H. Gu, Q. Lin, Modeling of smart composite box beams with nonlinear induced strain, Journal of Composites 30 (B) (1999) 603–612.
[18] C. Cesnik, S. Shin, On the twist performance of a multiple-cell active helicopter blade, Journal of Smart Materials and Structures 10 (1999) 53–61.
[19] A. Baz, J. Rao, Vibration control of rotating beams with active constrained layer damping, Journal of Smart Materials and Structures 10 (2000) 112–120.
[20] D. Hodges, E. Dowell, Non-linear equations of motion for the elastic bending and torsion of twisted nonuniform rotor blades, NASA TN D-7818, 1974.
[21] I. Chopra, T. Sivaneri, Aeroelastic stability of rotor blades using finite element analysis, NASA CR 166389, 1982.
[22] E. Smith, Vibration and flutter of stiff-inplane elastically tailored composite rotor blades, Journal of Mathematical and Computer Modeling, Special Edition on Rotorcraft Modeling, No 1 and 2 20 (1994).
[23] R. Ganguli, I. Chopra, Aeroelastic optimization of a helicopter rotor using two-cell composite blades, American Institute of Aeronautics and Astronautics Journal 34 (1996) 835–841.
[24] P. Inthra, F. Gandhi, Optimal control of helicopter vibration through cyclic variations in blade root stiffness, Journal of Smart Materials and Structures 10 (2001) 96–103.
[25] P. Friedmann, Rotary wing aeroelasticity with application to VTOL vehicles, Proceedings of the 31st AIAA/ASME/ASCE/ASC Structures, Structural Dynamics and Materials Conference, Long Beach, CA, April 2–4, 1990, pp. 1624–1667.
[26] A. Benjeddou, M. Trindade, R. Ohayon, Piezoelectric actuation mechanisms for intelligent sandwich structures, Journal of Smart Materials and Structures 9 (1999) 328–335.
[27] C. Sun, X. Zhang, Use of thickness-shear mode in adaptive sandwich structures, Journal of Smart Materials and Structures 4 (1995) 202–206.
[28] A. Benjeddou, M. Trindade, R. Ohayon, New shear actuated smart structure beam finite element, American Institute of Aeronautics and Astronautics Journal 37 (1999) 378–383.
[29] W. Chen, A. Saleeb, Constitutive Equations for Engineering Materials, Vol. 1: Elasticity and Modeling, Wiley-Interscience, USA, 1952.
[30] C. Lin, C. Hsu, H. Huang, Finite element analysis on deflection control of plates with piezoelectric actuators, Journal of Composite Structures 35 (1996) 423–433.
[31] J. Epps, R. Chandra, The natural frequencies of rotating composite beams with tip sweep, Journal of American Helicopter Society 41 (1996) 29–36.
[32] R. Ganguli, I. Chopra, W. Weller, Comparison of calculated vibratory rotor hub loads with experimental data, Journal of American Helicopter Society 43 (1998) 312–318.
[33] R. Ganguli, Optimum design of a helicopter rotor for low vibration using aeroelastic analysis and response surface model, Journal of Sound and Vibration 258 (2002) 327–344.
[34] C. Park, C. Walz, I. Chopra, Bending and torsion models of beams with induced-strain actuators, Journal of Smart Materials and Structures 5 (1995) 98–113.

[35] Piezo Systems, Inc., 186 Massachussets Avenue, Cambridge, MA.
[36] G. Surace, V. Anghel, C. Mores, Coupled bending–torsion vibration analysis of rotating pretwisted blades: an integral formulation and numerical examples, Journal of Sound and Vibration 206 (1997) 473–486.
[37] O. Song, N. Jeong, Vibration and stability of pretwisted spinning thin-walled composite beams featuring bending–elastic coupling, Journal of Sound and Vibration 237 (2000) 513–533.
[38] H. Yoo, J. Kwak, J. Chung, Vibration analysis of rotating pre-twisted blades with a concentrated tip mass, Journal of Sound and Vibration 270 (2001) 839–853.